

XMM-Newton Observation of the α Persei Cluster

Ignazio Pillitteri

*Smithsonian Astrophysical Observatory, MS 6, 60 Garden St., Cambridge, MA 02138; email
ipillitteri@cfa.harvard.edu*

Nancy Ramage Evans¹

*Smithsonian Astrophysical Observatory, MS 4, 60 Garden St., Cambridge, MA 02138; email:
nevans@cfa.harvard.edu*

Scott J. Wolk

Smithsonian Astrophysical Observatory, MS 70, 60 Garden St., Cambridge, MA 02138

Megan Bruck Syal

Department of Geological Sciences, Brown University, Box 1846, Providence, RI 02912

ABSTRACT

We report on the analysis of an archival observation of part of the α Persei cluster obtained with *XMM-Newton*. We detected 102 X-ray sources in the band 0.3-8.0 keV, of which 39 of them are associated with the cluster as evidenced by appropriate magnitudes and colors from 2MASS photometry. We extend the X-ray Luminosity Distribution (XLD) for M dwarfs, to add to the XLD found for hotter dwarfs from spatially extensive surveys of the whole cluster by ROSAT. Some of the hotter stars are identified as a background, possible slightly older group of stars at a distance of approximately 500 pc.

Subject headings: X-rays, stars, star activity, Alpha Persei

1

1. Introduction

Open clusters have been a keystone in understanding stellar evolution because they contain stars at the same distance with similar reddening formed at the same time with the same chemical

¹Corresponding Author

composition, at least to a first approximation. Their members display a range of masses, temperatures, luminosities, rotation rates, and multiplicity which can be explored. Comparison of cluster morphology provides an age sequence as a context for the evolution of stars. The well-known spin-down of low mass stars with age due to magnetic braking provides a good example of insight from clusters. This slowing of rotation results in the decrease of coronal X-rays due to their connection with stellar dynamos. Good summaries of the decrease in stellar activity as stars age for a range of masses are provided by Favata and Micela (2003) and Güdel (2004).

α Per is a young open cluster, found to be 50 Myr old from upper main sequence turnoff morphology (Meynet, Mermilliod, and Maeder, 1993). More recently, Stauffer, et al. (1999) have found an age of 90 Myr from the low mass lithium depletion boundary. Although there is some dispersion in the exact calibration of the age of the cluster, the sequence of age (increasing from the Orion Nebula Cluster through the α Per cluster through the Pleiades) is generally agreed. Thus, studies find a range in age from 50 to 90 Myr. We will use the shorthand “50 Myr” for the age of the cluster.

This age makes it an excellent comparison for Cepheids and their companions. Indeed, α Per itself is a yellow supergiant, with similar parameters to Cepheids, except for its location at a temperature outside the instability strip. As an example of usage of the cluster, we have observed a number of Cepheids with the Hubble Space Telescope Wide Field Camera 3 to identify a population of resolved low-mass stars close to Cepheids which are probable physical companions. X-ray observations showing an activity level comparable to that of α Per dwarfs would confirm that they are young companions rather than chance alignments with old field stars (e.g. Evans, et al. 2012). Another interesting aspect of a cluster of this age is that it is the period when young planets have just finished forming, and thus we gain insight into the X-ray environment during the early formation of atmospheres.

Because the cluster is nearby, it covers a wide area in the sky. It was observed with a raster of pointings by *ROSAT* (Randich, et al. 1996). Essentially all the late F, G, and K members from the membership studies of Prosser (1992) were detected. Three deeper pointed *ROSAT* observations (22-25 ks) were subsequently made covering part of the cluster (Prosser, et al. 1996). Two additional studies were made using near IR observations to try to identify counterparts of *ROSAT* sources (Prosser and Randich 1998; Prosser, Randich, and Simon 1998, PRS below). In the second of these, the authors identified a number of G and K stars with lower X-ray luminosity than expected for cluster members, which they termed “bad L_X stars”. Finally, a deeper (60 ksec) exposure of a small part of the cluster was made with XMM, which was described briefly by Pallavicini, Franciosini, and Randich (2004). This is the observation which we discuss here, which allows us to investigate fainter sources as well as the spectral properties of the sources. In addition to being relatively nearby (170 pc; Randich, et al. 1996), the α Per cluster is also lightly reddened ($E(B-V) = 0.09$ mag; Meynet, et al. 1993), making the data interpretation relatively robust.

The supergiant α Per itself was detected in the *ROSAT* observations (Prosser, et al. 1996).

However, recently Ayres (2011) has suggested that there is evidence that the X-rays might actually be produced by a low-mass X-ray active companion.

In this study we add the results of the deeper XMM image to the existing literature on the cluster. Specifically, in the sections that follow, we discuss the observations, the source detection and near IR matches, the source parameters (luminosity and spectra), the X-ray luminosity distribution (XLD), light curves, and the results. Of particular importance in deriving the cluster parameters (Discussion section, Section 4) is a grouping of stars likely to be a cluster of young stars behind the α Per cluster.

2. Observations and Data Analysis

A fraction of the α Per cluster was observed by XMM-Newton as part of the Mission Scientist Guaranteed Time (Pallavicini, et al 2004). A 60 ks observation was obtained in Sept 5th 2000-09-05 using EPIC MOS and PN cameras on board *XMM-Newton* with a pointing at R.A.: $3^h26^m16^s$ and Dec.: $48^d50^m29^s$. Fig. 1 shows the composite PN, MOS 1 and MOS 2 image of the EPIC field within the α Per cluster.

We carried out Data Analysis similar to that in Pillitteri, et al. (2004). We used the standard tasks of SAS v10.0 to reduce the *ObservationDataFiles* (ODF) and obtain event tables calibrated in arrival time, energy and astrometry. First the events were filtered to be within the band 0.3–8.0 keV, appropriate for the coronal emission we want to investigate. Good time intervals (GTIs) were filtered out after inspecting the light curve of events at energies higher than 10 keV ² and removing high background intervals (with rate thresholds of >2.5 ct s⁻¹ for PN and >0.5 ct s⁻¹ for MOS). This optimizes the event lists for the detection of faint X-ray sources.

²See http://xmm.esac.esa.int/sas/current/documentation/threads/EPIC_filterbackground.shtml

Table 1: List of X-ray sources detected in EPIC-*XMM-Newton* image. The first five rows are shown here; the complete table is available in electronic form.

ID	R.A. J2000	Dec. J2000	Offaxis '	Rate cts/ks	Err cts/ks	Exposure Time ks
1	03:26:37.9	48:37:28.9	15	15.7	5.55	48.3
2	03:25:43.7	48:38:32.4	14	7.76	1.63	50.7
3	03:26:43.6	48:38:47.7	14	6.75	1.66	57.3
4	03:26:01.3	48:39:10.1	12	21.7	4.83	59.9
5	03:25:50.9	48:39:22.2	13	29.4	7.41	57.4

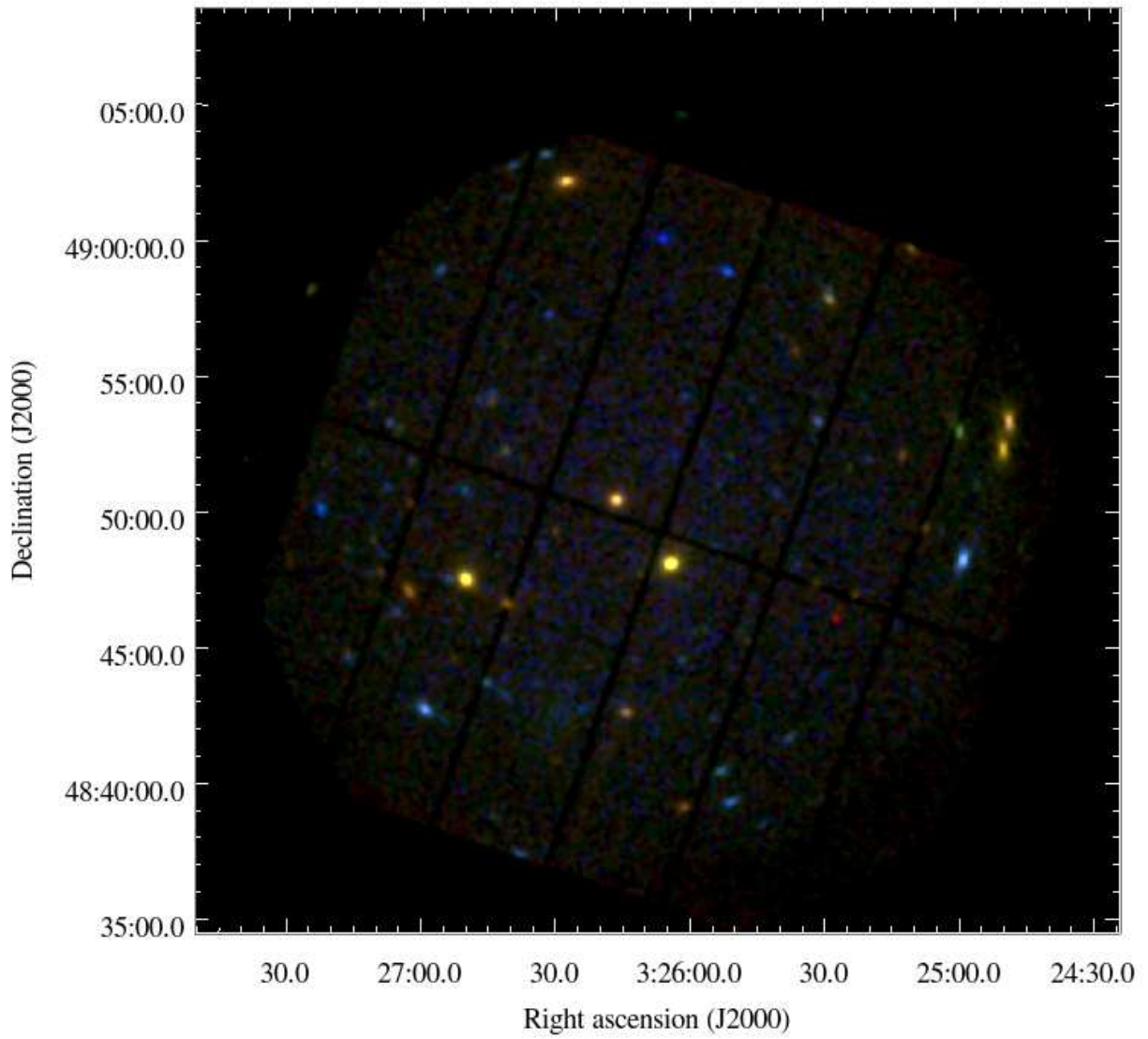


Fig. 1.— Composite PN Mos 1 Mos 2 *XMM-Newton* image within the α Per field. The bands used are: Red= 0.3 – 1.0 keV, Green= 1.0 – 2.5keV, Blue = 2.5 – 8.0 keV.

2.1. Source Detection

Source detection was performed using the algorithm based on wavelet convolution described in Damiani et al. (1997a,b) and optimized for *XMM-Newton* (Pillitteri et al. 2004). The threshold used for positive detection of sources was 4.8σ above local background fluctuations.

The full list of source parameters is provided in Table 1 in the electronic version. The first few entries are provided in the hardcopy illustrate the content. The columns of the table list the source number, right ascension, declination, distance off axis, source count rate, and effective exposure time (for the summed MOS and PN detectors, assuming a PN–MOS conversion factor of 3.1). We detected 102 sources in 0.3–8.0 keV band.

2.2. Optical Catalogs

We have cross-correlated the positions of X-ray sources with the optical catalogs of Prosser (1992), Randich, et al (1996) and Deacon and Hambly (2004) with a match radius of $5''$. Only one object of the catalog by Prosser is in the main field of view of XMM but was not detected. Another object from that catalog is on the edge of the XMM field and was also undetected. Two objects of the Deacon and Hambly catalog are detected in X-rays, and four stars from the Randich et al. catalog are matched with X-ray sources. We have used the 2MASS catalog (Cutri, et al. 2003) to find near IR counterparts to the X-ray sources, finding 39 matches (Fig. 2). X-ray sources detected on the image (Fig. 1) are a mixture of active young stars from the α Per cluster and background objects. Any star more massive than M5 would have a K magnitude ≤ 13.6 at the age and distance of α Per (Siess, 2001). Therefore, we assume that sources without counterparts in the 2MASS catalog are distant active galactic nuclei (AGNs) which are too faint in the IR. Table 2 provides IR photometry for sources identified as stars within $5''$ of the position of X-ray sources, with with source number, coordinates, 2MASS ID, and J, H, and K magnitudes in successive columns. Parameters derived from fitting (kT, emission measure, and luminosity) are discussed below in Section 3.2. Note that in Table 2, X-ray luminosities have been computed from X-ray

Table 2: List of sources with 2MASS match and parameters from best fit modeling of X-ray spectra.

ID	R.A. J2000	Dec. J2000	2MASS ID	J mag	H mag	K mag	kT keV	E.M. cm^{-3}	$\log f_X$ $\text{ergs s}^{-1} \text{cm}^{-2}$	$\log L_X$ ergs s^{-1}
4	03:26:01.3	48:39:09.7	03260131+4839097	12.60	11.92	11.69	0.76	51.7	-13.8	28.8
10	03:26:14.2	48:42:38.3	03261419+4842382	12.48	11.80	11.56	0.89	51.9	-13.6	29
19	03:26:22.7	48:44:20.1	03262270+4844201	12.77	12.31	12.20	0.86	50.7	-14.9	27.7
22	03:26:52.6	48:44:37.9	03265263+4844378	11.10	10.77	10.76	0.88	51.1	-14.4	28.1
42	03:24:58.8	48:48:14.7	03245884+4848147	16.47	15.69	14.52	–	–	–	–

fluxes assuming the sources are at the distance of α Per. This is probably not true for the “bad L_X ” sequence (discussed in Sections 3.1 and 4 below).

3. Results

3.1. The X-ray Luminosity

The color–magnitude diagram from the 2MASS photometry is shown in Fig. 3. In it, the sources are numbered with the X-ray source ID (Table 1). The size of the circle is proportional to the X-ray luminosity, which is derived from the count rate using a conversion factor from *PIMMS* derived from a 1-T APEC spectrum with $kT=1$ keV and $NH = 10^{20}$ cm^{-3} . Overlaid on the figure is the isochrone from Siess et al. (2000) for an age of 50 Myr and solar metallicity. The figure shows the well-known decrease in X-ray luminosity with bolometric luminosity along the main sequence. The Siess tracks allow us to infer masses (see Sect. 3.3).

A second sequence below the main cluster sequence is present, near the shifted isochrone (dotted line) in Fig. 3. This sequence is made up of sources 19, 22, 25, 39, 58, 59, 62, 63, 67, and 87 in Table 2. For stars fainter than $J \simeq 14$ mag, the distinction between the two sequences is more ambiguous. However, referring to the morphology of the color-magnitude diagram in Lodieu, et al. (2012; Fig. 6) the main sequence is nearly vertical, and we accept the fainter stars as predominantly belonging to the cluster itself. The lower sequence appears to correspond to sources labeled “bad L_X ”, in PRS Fig. 5. These sources have a lower X-ray luminosity than the sequence of cluster members. We draw attention to the low-lying sequence in the near IR data (Fig. 3), and will discuss the characteristics of these stars in the succeeding sections. It is possible, of course, that some of the stars near the isochrone of the cluster are not in fact cluster members. Star 71, could for instance be a foreground star.

We have divided the stars in Fig 3 in a straightforward way to examine the dependencies of L_X . There is a significant gap between the cluster main sequence, and the lower sequence, the stars classified “bad L_X ”. Within the cluster sequence, stars have been grouped into “F-G”, “K-early M”, and “late M” according to gaps in the magnitude distribution. Fig. 4 shows the count rate as a function of J magnitude. The F-G stars (asterisks) and the K-M stars (triangles) show the well known progression to lower count rates for cooler stars. The exceptions are a few of the hottest F-G stars, suggesting that their convective envelopes and X-ray production are just becoming established. The bad L_X stars occur in a separate location, with lower count rates and fainter magnitudes, except that the faintest stars in both sequences which are mixed in the figure. Note that this is despite the fact that Fig. 3 shows that the “bad L_X ” stars are in general bluer than the K-M stars in the α Per sequence. Similarly, Fig. 5 shows the log count rate as a function of color. The “bad L_X ” stars clearly have lower count rates than cluster main sequence stars of comparable colors. Thus low count rate “bad L_X stars” have properties distinct from cluster members in both near IR photometry (Fig. 3) and in X-rays.

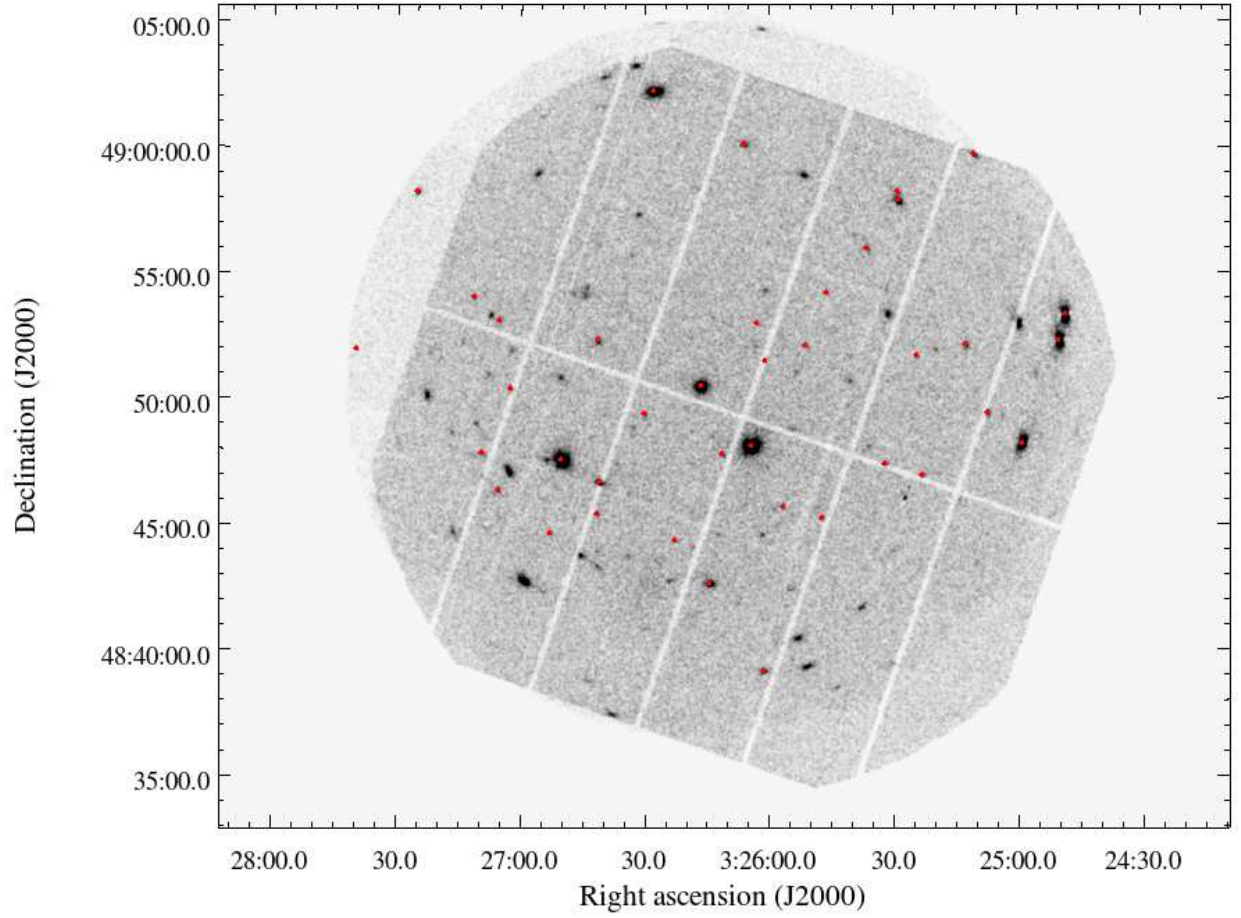


Fig. 2.— The combined PN, MOS1 and MOS2 XMM image with the 2MASS sources indicated in red; the stars from the Prosser catalog are in green.

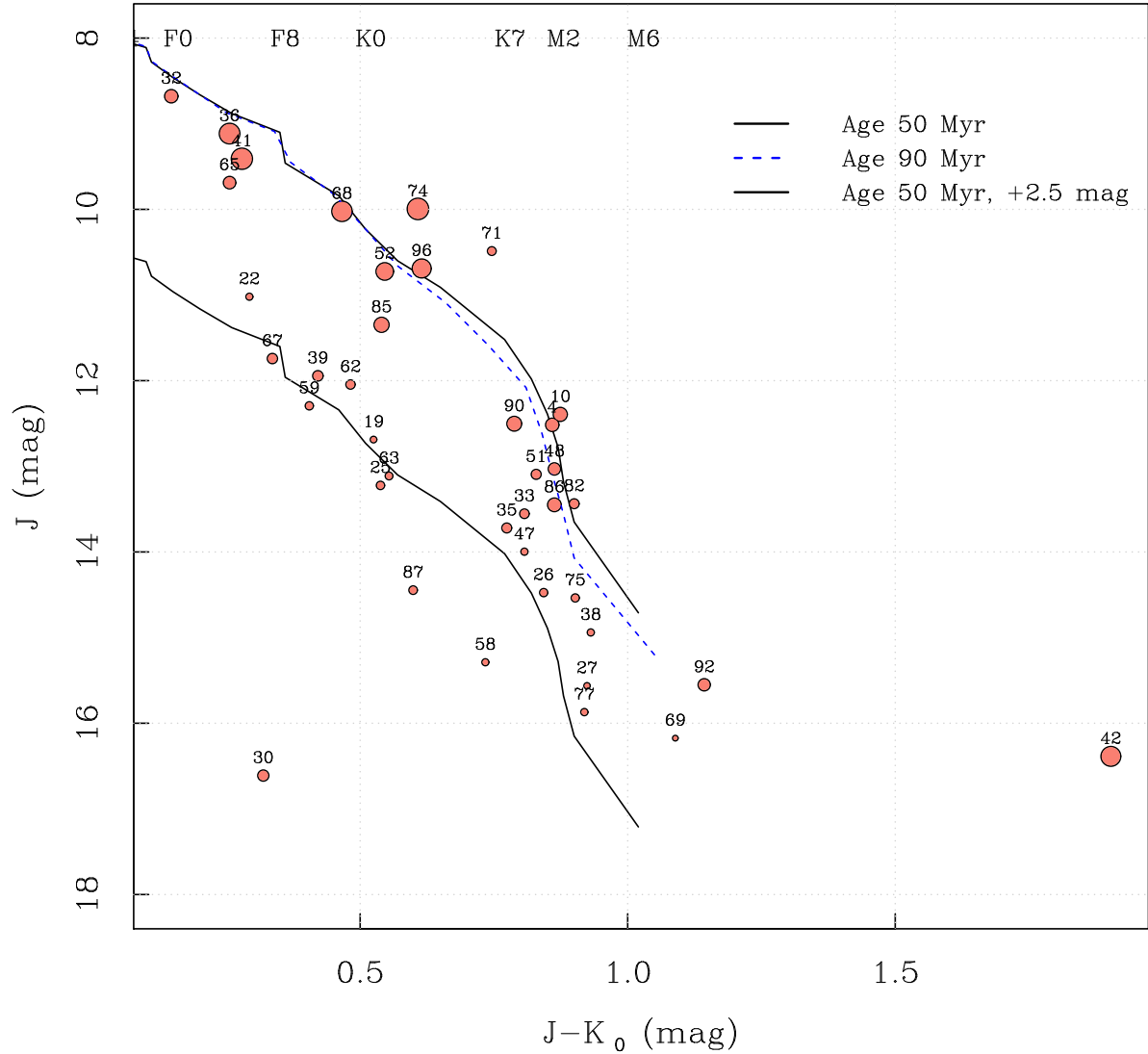


Fig. 3.— The 2MASS $J-(J-K)_0$ color magnitude diagram for the stellar X-ray sources. The circles are proportional to the strength of the X-ray signal. Spectral types for the $(J-K)_0$ colors are indicated on the top axis. The top upper solid line is the isochrone for 50 Myr age from Siess et al. (2000) for the distance of α Per. The dashed line just below that is the isochrone for 90 Myr. The solid line at the bottom is the same isochrone shifted by 2.5 magnitudes to match the “bad L_X sequence.”

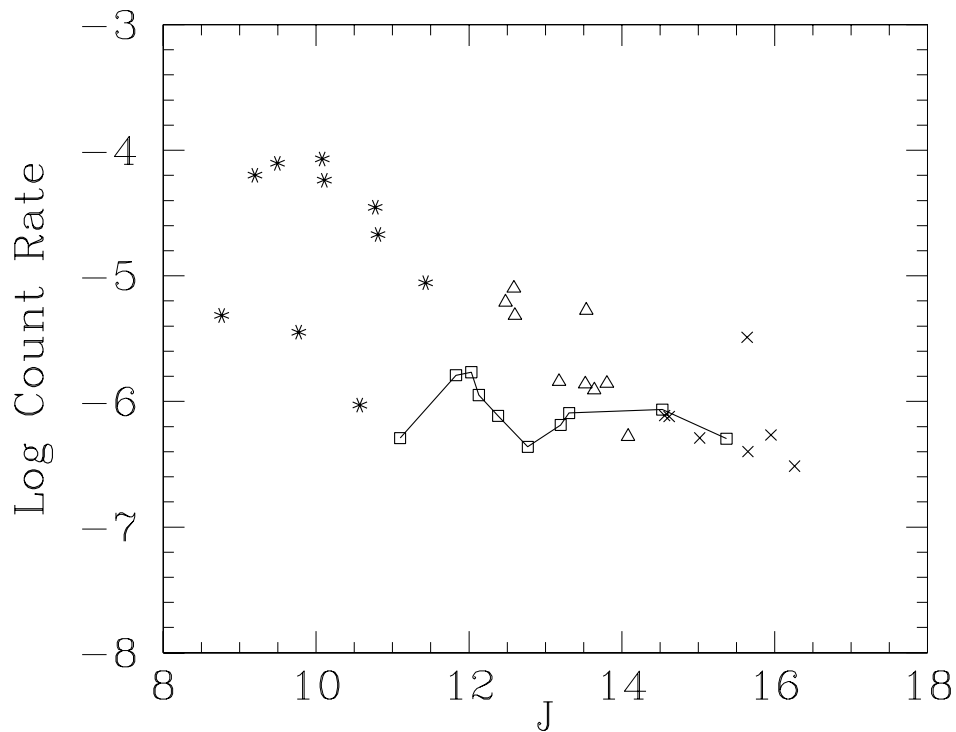


Fig. 4.— The log of the count rate as a function of J magnitude. Symbols are as follows: F-G stars: *; K-early M stars: triangles; late M stars: x; “bad L_X ” stars: squares. To emphasize the location of the “bad L_X ” stars, they have been connected in order of magnitude. Two distinct sequences are seen, merging at the faintest stars. J is in magnitudes, count rate is counts per ksec.

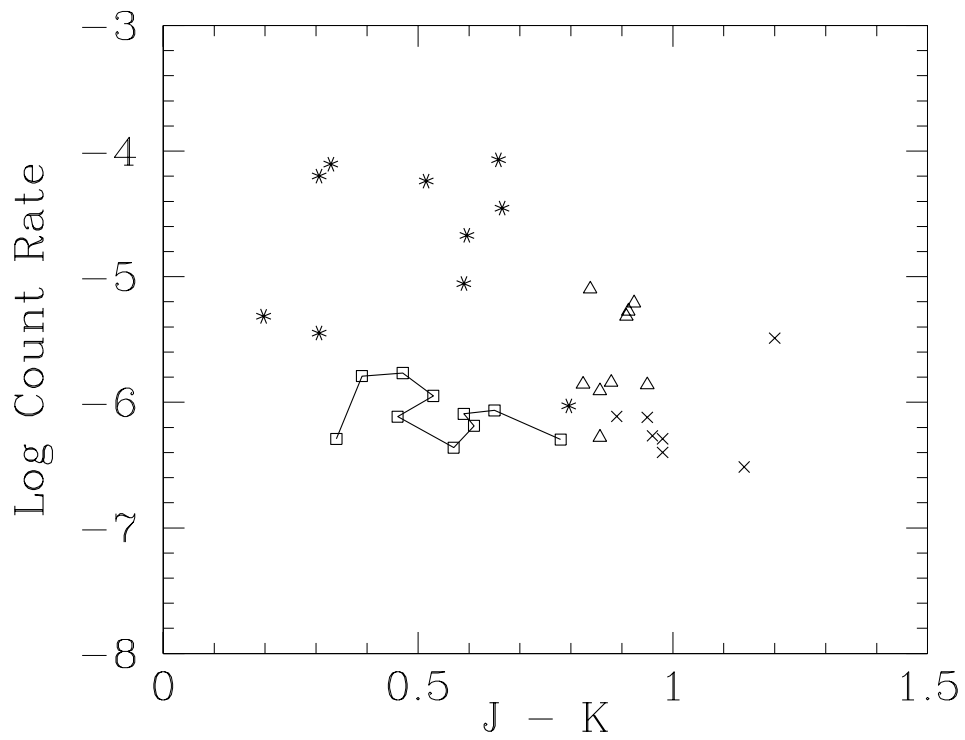


Fig. 5.— The log of the count rate as a function of J-K color. Symbols are the same as Fig. 4. The “bad L_X ” stars clearly have lower count rates than cluster main sequence stars of the same color. J-K is in magnitudes, count rate is counts per ksec.

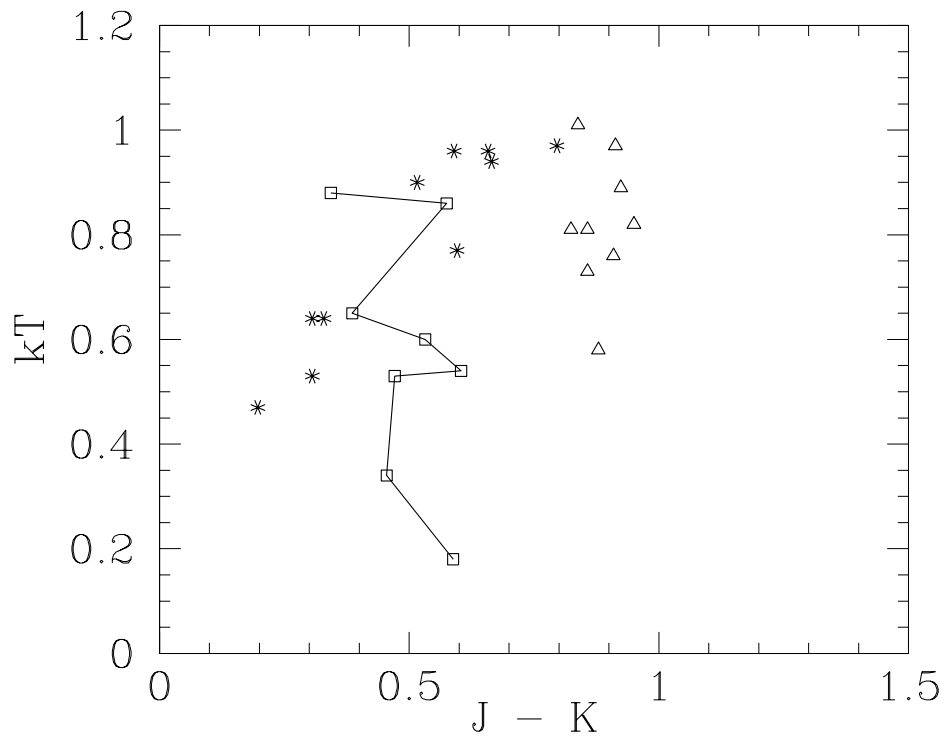


Fig. 6.— The temperature kT (keV) as a function of the J-K color. Symbols are the same as in Fig. 4, except that the “bad L_X ” stars are linked in order of kT . J-K is in magnitudes, kT is keV.

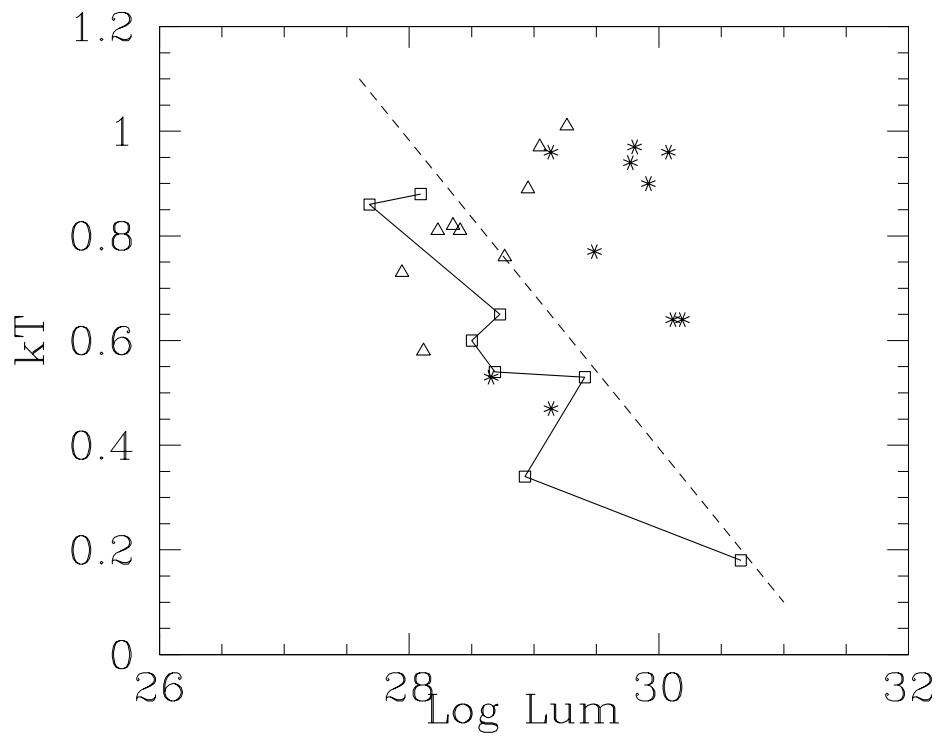


Fig. 7.— The temperature kT (keV) as a function of X-ray luminosity. Symbols are the same as in Fig. 6. The dotted line is the upper envelope below which the bad L_X stars fall. Luminosity is in $\text{ergs cm}^{-2} \text{s}^{-1}$.

3.2. Spectra

One of the most important parameters to examine for the cluster stars is the temperature derived from the X-ray spectra. In order to use temperature from a large number of sources, we have made 1 temperature fits of *APEC* models to the spectra with *XSPEC* software (ver 12.6). These temperatures are listed in Table 2. For low countrates, we did not fit spectra, and the temperature, emission measure, flux and luminosity columns in Table 2 are blank. These sources are omitted from figures. (Luminosities in Fig. 3 were derived as in section 3.1 assuming $kT = 1$ keV.) Fig. 6 shows the temperatures for the groups of stars as a function of the J-K color. The late M stars in Figs 4 and 5 are all too weak to have a reliable temperature determination. All groups (the F-G stars, the K-M stars and the bad L_X stars) have a range to temperatures. However the mean X-ray temperature kT for the bad L_X stars (0.57 keV) is lower than the mean for the other 2 groups (0.80 keV). Fig. 7 shows the X-ray temperature as a function of luminosity for all groups. The luminosity is computed on the assumption that all the stars are at the cluster distance. Both the F-G and K-M stars show a range of temperatures along with the well-known decrease in X-ray luminosity for the lower mass stars. These two groups exhibit minimal overlap in the figure and a large dispersion. The dotted line indicates the upper envelope of the bad L_X stars, which do not in general reach the highest luminosities of the other groups.

To illustrate the effects of different source temperatures, Fig. 8 shows the spectra of two strong sources, Src 68 and Src 36. Src. 36 is an F star ($J = 9.2$ mag) with a single temperature fit (Table 2) $kT = 0.64$. Src 68 has $J = 10.11$ mag, and $kT = 0.9$. The softer spectrum of Src 36 is clearly apparent in Fig. 8.

For about half the strong sources, the χ^2 was satisfactory for a single temperature fit. For the other sources, Table 3 lists the temperatures for 2 temperature fits, together with the off-axis distance and source counts. Source counts include all 3 cameras (MOS1, MOS2, AND PN) taking into account the different effective areas of the 3 cameras. Fig. 9 shows the results. A correlation between the two temperatures is present, as found by Wolk, et al. (2005) and Briggs and Pye (2003). In order to investigate this relation as a function of age, Fig. 9 includes data from the 1-3 Myr Orion Nebula Cluster (ONC) COUP project (Wolk, et al. 2005), the 100 Myr Pleiades (Briggs and Pye 2003) and 30 Myr NGC 2547 (Jeffries, et al. 2006) as well as fits to XMM ONC sources (Table 4) to explore this with XMM and Chandra data. ONC Chandra data were taken from Wolk, et al. for the “characteristic flux” (their Table 4), omitting the data for the 4 stars flagged as poor fits. Their fit to that data ($kT_2 = 2.14 \times kT_1 + 0.660$ keV) is also included in Fig. 9. Data for the Pleiades were taken from the XMM observations of Briggs and Pye (2003), using the two temperatures from the PN (their Table 3), since only one source had determinations for several instruments, and they are all similar.³ We also include 9 sources from the 30 Myr cluster NGC 2547 (Jeffries, et al. 2006). Data for NGC 2547 is taken from the 2 temperature fits

³Daniel, Linsky, and Gagne (2002) also fit Chandra spectra of several sources, but kT_2 was fixed in their solutions.

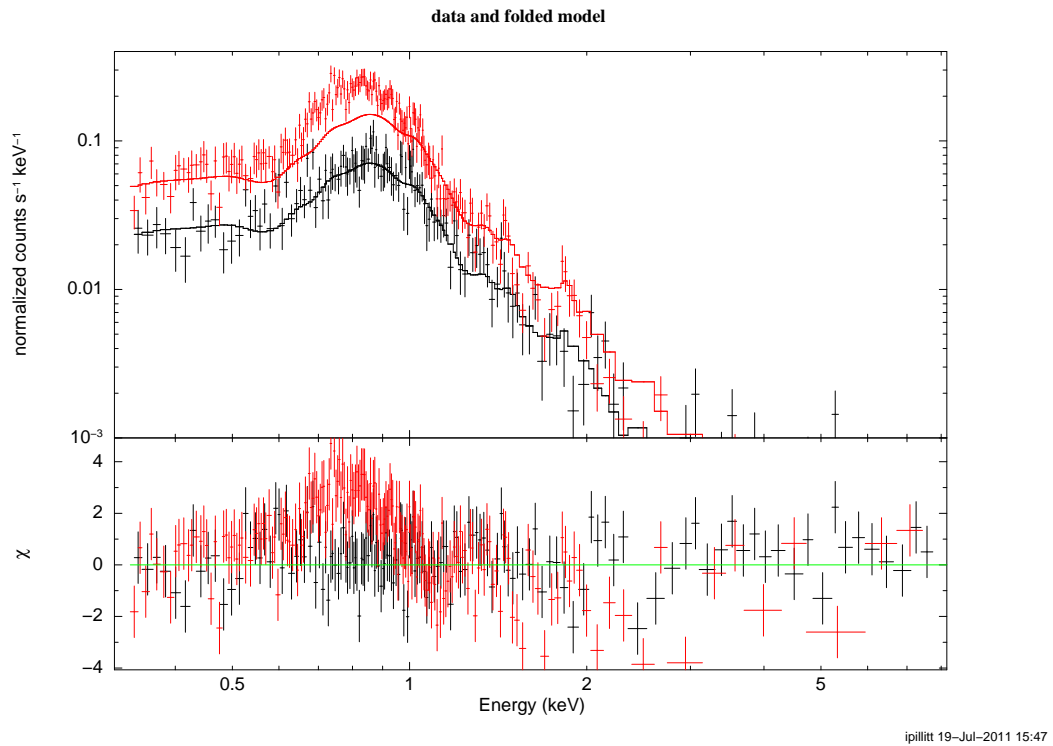


Fig. 8.— Spectral fits of sources 68 and 36. Top: Src 68 is in black; Src 36 is in red. The red line is the spectral fit to Src 68 shifted upward for comparison with Src 36. Excess soft flux in the spectrum of Src 36 is clearly seen in comparison with the fit to Src 68. Bottom: Residuals from the fit in the same colors as the top.

in Jeffries, et al. (2006; their Table 5), omitting sources where kT_2 is described as unconstrained in the fits. Sources which are late B stars (#7 and #8) were also omitted. However, their two temperatures match those of the cool stars very well, confirming that the X-rays from these sources come from a low-mass companion.

Fig. 9 shows that both the kT_1 and kT_2 temperatures are smaller on average for the 50 Myr α Per stars than for the younger ONC stars (1-3 Myr; Megeath, et al. 2012). This is expected as a result of the decrease in stellar activity as stars age. (The single point for α Per with $kT_2 > 2$ is for a source which is both weak compared to the others and off axis, and hence has a significant systematic error in addition to the measurement error.) The Pleiades stars (100 Myr) fall among the α Per stars, but the hottest of both kT_1 and kT_2 for Pleiades stars is cooler than those for the α Per stars. Similarly, the NGC 2547 stars (30 Myr) largely overlap the α Per stars. The lines at the bottom of Fig. 9 indicate the range of kT_1 values ordered from the youngest cluster (ONC) to the oldest (the Pleiades). This shows the decrease in stellar activity as stars age. Once on the Zero Age Main Sequence (ZAMS), rotation and hence dynamo activity decreases as stars spin down. Jeffries et al. discuss activity at 30 Myr in NGC 2547 for G, K, and M stars. At this age, solar mass stars have just contracted to the ZAMS. They argue that coronal temperatures decrease up to this point as gravity increases. The decrease in the harder component in solar mass stars was previously noted by Güdel, Guinan, and Skinner (1997) and subsequently by Telleschi, et al. (2005)

There is a correlation between kT_1 and kT_2 in Fig. 9, particularly for α Per and the ONC. There is a suggestion, however, that the relation for α Per is less steep than for the ONC. That is, even for the same soft component temperature kT_1 , the hard component decreases as stars age. The Pleiades stars (100 Myr) cluster among the α Per stars, although the coronae appear generally cooler than the α Per sample and there appears to be much less differentiation among the individual stars, with 5 of the 8 being well described as $kT_1 = 0.35 \pm 0.050$ keV and $kT_2 = 0.950 \pm 0.100$ keV. Due to this clustering no slope can be determined for the Pleiades stars. In fact the concept may no longer be relevant at that age if the hot component is gone. Typically older cool stars have a corona that is dominated by a one-temperature cool plasma. If the cool component at 100 Myr has already reached this asymptotic minimum, then these stars may be best described merely a single temperature which is a function of time.

This discussion, of course, is produced from a sample for all clusters that is biased in the sense that the two temperature fits are only possible for the strongest X-ray sources. In addition, in the α Per cluster, a number of strong sources are satisfactorily fit with one temperature. Furthermore, the samples from different clusters may contain a different distribution of spectral types, again creating possible bias.

Table 3: Two Temperature Fits for the α Per Cluster

Src	kT ₁ keV	kT ₂ keV	Off Ax "	Cts
4	0.18	0.88	12	289
36	0.5	0.86	8.1	7030
41	0.46	0.9	3.5	10200
52	0.24	0.98	1.8	3170
68	0.77	1.42	13	2100
74	0.81	1.48	13	2380
85	0.74	1.52	9	651
90	0.81	2.6	12	279
96	0.57	1.24	11	2520

Table 4: Two Temperature Fits for the ONC (XMM)

Obsid	Src	kT ₁ keV	kT ₂ keV
0212480301	304	0.97	2.49
0093000101	281	0.78	1.86
0212480301	221	0.30	1.58
0212480301	237	0.51	1.33
0212480301	280	0.81	1.57
0093000101	281	0.78	1.86
0093000101	229	0.84	1.76
0093000101	200	0.73	1.86
0093000101	194	0.96	2.14
0093000101	196	0.25	1.30
0093000101	309	0.20	0.99
0093000101	132	1.04	3.71
0093000101	158	0.25	1.02

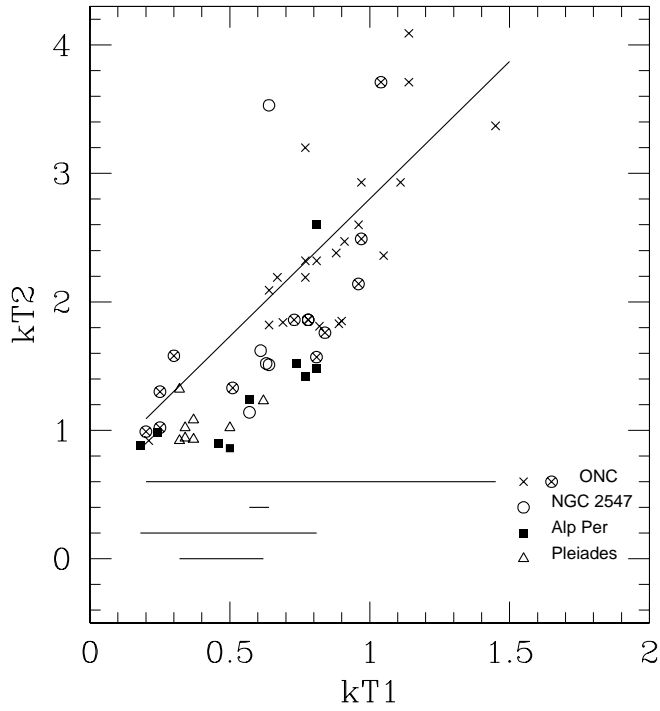


Fig. 9.— The two temperatures from spectral fits, kT_1 and kT_2 . α Per stars are shown by filled squares, Orion Nebula Cluster sources from Wolk et al. (2005) by x's, XMM Orion Nebula Cluster sources (Table 4) by circled x's; Pleiades stars by open triangles and NGC 2547 by open circles. The line is the fit to the Wolk et al. Orion data. Beneath the plot the range of the kT_1 for each cluster is shown, from the youngest cluster (the ONC) to the oldest (the Pleiades). kT_1 and kT_2 are in keV.

3.3. X-ray Luminosity Distribution (XLD)

Although the XMM field covers only a small part of the α Per cluster, the exposure is deeper than the ROSAT images. We derive an X-ray luminosity distribution (XLD) to compare with the ROSAT results for the full cluster area using the *ASURV* software package. As discussed in Sect. 2.2, there are two sequences. The brighter sequence is from the cluster itself. There is also a fainter sequence, corresponding to the “bad L_X ” stars, which will be discussed further in Section 4. The XLD is derived from the upper cluster sequence. Fig. 3 shows that it contains a natural divide in the J–(J–K)₀ diagram, with a gap in both color and magnitude. The sources 32, 36, 41, 52, 65, 68, 71, 74, 85, and 96 in Table 2 belong to the earlier side of the low-mass main sequence stars (G–K stars). Others in that sequence are assigned to the cooler low-mass star group (M stars). The division in (J–K)₀ comes at the end of the K dwarf color, so the first group contains F, G, and K stars. Since the number of sources in the part of the cluster we are sampling is small, we are not able to subdivide this group further. The cooler group contains M stars. Since we do not have a list of authenticated faint cluster members, we do not have upper limits for nondetections of faint members. Fig. 10 provides the results. The luminosity distribution for the F, G, and K stars is similar to the results from Randich, et al. (1996) for the full cluster. For instance, the mean $\log L_X$ from that study is 29.63 ergs sec^{–1} (F dwarfs), 29.74 ergs sec^{–1} (G dwarfs), and 29.56 ergs sec^{–1} (K dwarfs), comparable to the blue line in Fig. 10. For the M dwarfs, the deeper XMM data provide a distribution that continues more smoothly to lower luminosities than the Randich, et al. distribution which has a mean $\log L_X$ of 28.96 ergs sec^{–1}. For completeness, we derive an XLD for the “bad L_X ” distribution as though it were at the same distance as the cluster even though this is likely an incorrect assumption (see Section 4). Thus, the XMM results for the α Per cluster are in agreement with the previous ROSAT results for the XLD for F, G, and K stars, but they extend the XLD to fainter sources for M stars. Fig. 10, for instance provides a basis for inferring the properties of possible low-mass companions of Cepheids (Evans, et al. 2012), necessary for calculating X-ray exposure times.

3.4. X-ray Time Variability

We have examined the light curves of the sources to look for time variability, since flares are expected at the young age of α Persei cluster. However because most of the sources have relatively low counts and 60 ksec is a short interval, we discuss here only six bright sources that show possible variability in inspection by eye. Fig. 11 shows the PN light curves of these bright sources, all of which belong to the “cluster” sequence. Source 36 shows a smooth rise of about 1 σ level and a flare-like event at 43 ks. The flare has peak rate 50% larger than the pre-flare rate and a significance $> 2 \sigma$. The duration is 3–4 ks. Other possible small flares are visible at about the 1 σ level. Sources 41, 68, and 96 are largely constant, with possible variability at the 1 σ level. Source 74 shows a possible sequence of flares, the first at $\simeq 13$ ks with a duration of 8 ks and peak rate about 80% larger than minimum observed rate. Source 90 is interesting because it has a very low

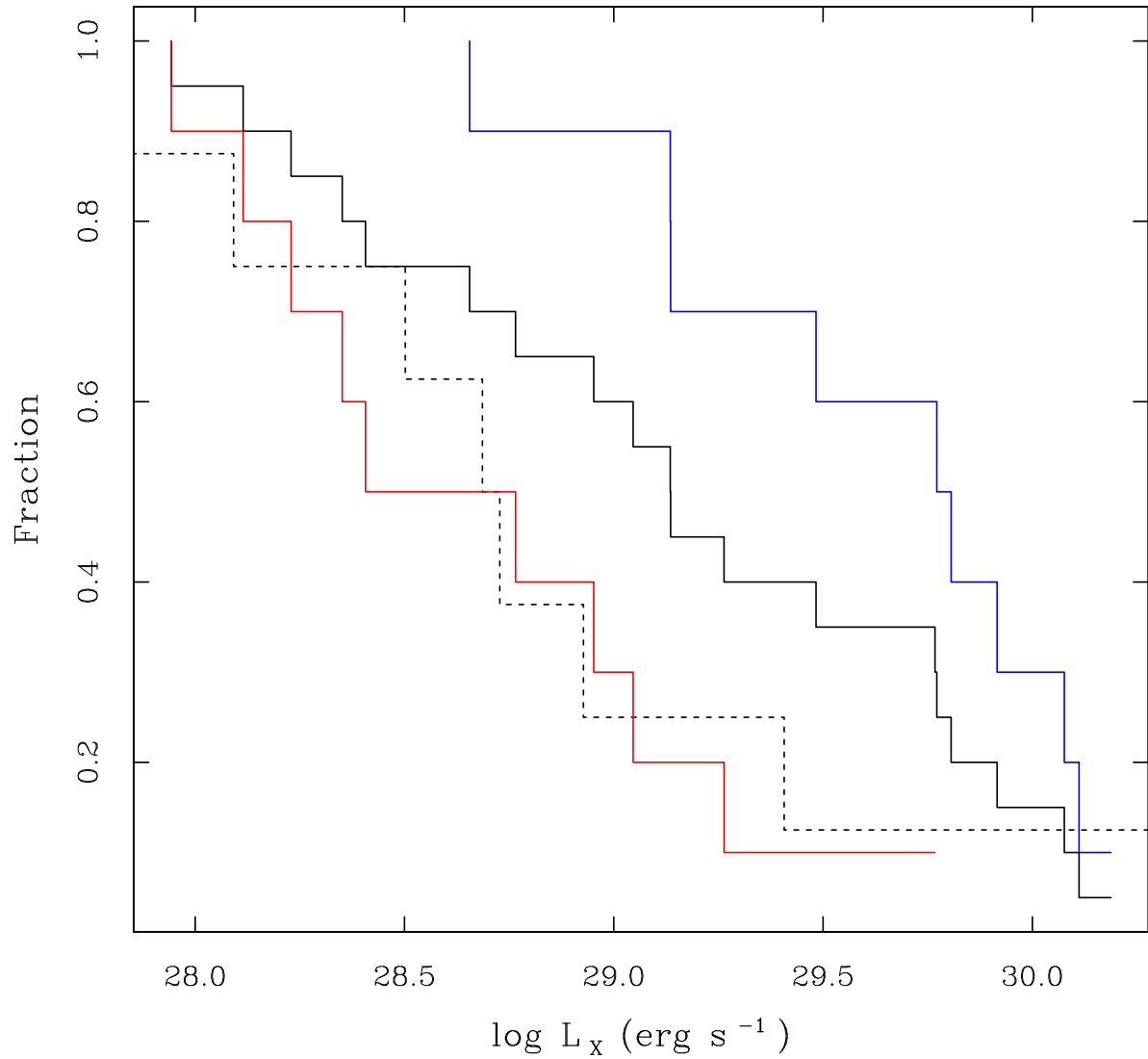


Fig. 10.— The X-ray Luminosity Distribution (XLD). The black solid line is for the all spectral types; the blue solid line is for the hotter of the low-mass main sequence stars; the red solid line is for cooler main sequence stars; the dotted line is for the “bad L_X ” stars, assuming they are at the distance of the cluster (see text for discussion).

count-rate in the first half of the observation, then a slow increase and a steeper fall within 10 ks. The peak rate in this event is about 8 times the quiescent rate. In summary, in the brief window of the observation, several sources show evidence of low level variability, but only one has a significant flare.

4. Discussion: Bad L_X Sources

We have used the deep XMM exposure of the α Per cluster to sample the XLD of a section of the cluster. In particular we have added a sample of M stars to the previous work. This confirms that the distribution fits nicely between the youngest clusters (e.g. the Orion Nebula Cluster) and the older Pleiades.

An unusual feature of both the ROSAT and the XMM images of the cluster is the additional sequence, dubbed the “bad L_X ” stars by PRS. It was first identified in the ROSAT images, however it is clearly evident in the near IR color-magnitude data of the XMM X-ray sources (Fig. 3) as well. The simplest explanation is the geometric one, that the “bad L_X ” sequence comes from a more distant grouping behind the α Per cluster. Interpreting Fig. 3 in this way, the sequence is 2.5 magnitudes fainter than the α Per sequence as shown by the shifted isochrone in Fig. 3, which translates into a factor of 3 further in the distance, making it about 500 pc away. This ignores possible additional reddening at that distance. However, the faintest pair of stars in the “bad L_X ” sequence are in the late-K and M region where the main sequence in Fig. 3 is nearly vertical. Their $(J-K)_0$ is not consistent with significant additional reddening as compared with the cluster sequence. The increase in the “bad L_X ” distance of 3 implies an addition of 1. to the $\log L_X$ or \log count rate. Fig. 5 provides a good check on this possibility. Even if the \log count rate were adjusted by this amount, it would still fall a little below the α Per sequence for the same J-K. This suggests that the grouping may also be a little older than the 50 Myr α Per cluster. There is evidence for this in Fig. 6, in that the average kT (in the relevant J-K band) is a little smaller than for the α Per stars with the same colors. Thus there is a suggestion in Fig. 6 that the “bad L_X ” stars may be slightly older than the α Per stars. However there are only 8 stars and several parameters involved (distance, reddening, age/temperature) so this is not a conclusion, rather a possible interpretation of the available data. For a second comparison, in Fig. 10, if the estimated addition to the “bad L_X ” of 1. is subtracted from the $\log L_X$ of the F-G-K stars of the cluster (blue line), it would be moved nearly to the $\log L_X$ LXD (dotted line). It is not surprising from Fig. 3 that faint M stars are not detected at the distance of the “bad L_X ”, and hence the F-G-K stars (blue line) are the best comparison at that distance. While the small number of “bad L_X ” stars preclude firm conclusions, we at least offer a plausible interpretation of a group about the same age as the α Per cluster or possibly a little older.

PRS remarked that the “bad L_X ” stars are frequently classified as nonmembers of the α Per cluster on the basis of radial velocities. Of the 7 “bad L_X ” in their Table 4 with radial velocities, 5 are listed as nonmembers on the basis of radial velocities, and for the other two, the membership

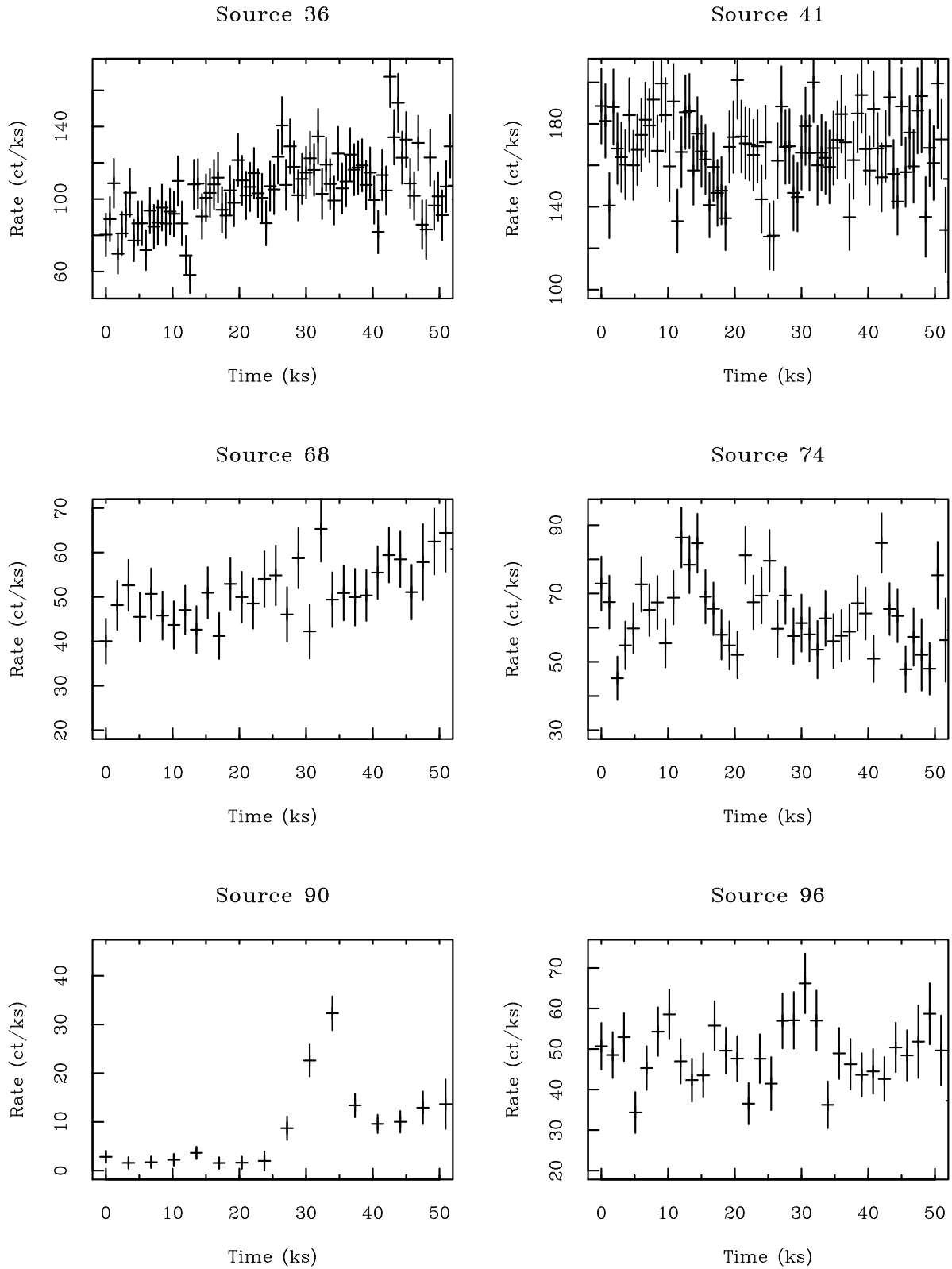


Fig. 11.— Light Curves for a selection of brighter sources. See text for discussion.

status is questionable.

There is one restriction on the distance of the “bad L_X ” stars, which is that they cover a large part of the α Per area surveyed by PRS. That is, it cannot be so much further behind that it covers only a small fraction of α Per cluster area, which is quite extended on the sky. However, α Per cluster members have been found in ground-based studies in an area on the sky about twice as wide at the PRS ROSAT observations (Prosser 1992). Thus a grouping about twice as far away as the α Per cluster is consistent with the spread of “bad L_X ” stars on the sky.

In summary, a grouping behind the α Per cluster is a plausible explanation for the “bad L_X ” sequence. This interpretation is key to deriving a XLD appropriate for the 50 Myr stars in the α Per cluster itself.

5. Summary

We have investigated an archival XMM-Newton image of part of the α Per cluster, partly because the age of this cluster makes it appropriate for comparison with low-mass companions of Cepheids. In particular, this data adds observations of X-ray faint M stars to the wider but shallower observations of the whole cluster area by ROSAT. The count rate sequence for the M stars continues the sequence for hotter dwarfs in both J magnitude and J–K color. XLD’s have been derived for both the hotter dwarfs, and also the M stars. The “bad L_X ” sequence identified by PRS appears to be a background grouping at a distance of about 500 pc and an age similar (or slightly older) than the α Per cluster, as shown by near IR magnitudes and colors, as well as X-ray luminosities and temperatures.

IP is grateful to Dr. E. Franciosini for providing an unpublished catalog of members of Alpha Persei. We thank an anonymous referee for comments that improved the presentation of the paper. The XMM-Newton guest investigator program supported IP through grant NNX09AP46G. Support for this work was also provided from the Chandra X-ray Center NASA Contract NAS8-03060. VizieR and SIMBAD were used in the preparation of this study.

REFERENCES

- Ayres, T. R. 2011, *ApJ*, 738, 120
- Briggs, K. R. and Pye, J. P. 2003, *M. N. R. A. S.*, 345, 714
- Cutri, R. M., Skrutskie, M. F., van Dyk, S., et al. 2003 *VizieR Online Data Catalog* 2246, 0
- Damiani, F., Maggio, A., Micela, G., and Sciortino, S. 1997a *ApJ*, 483, 350
- Damiani, F., Maggio, A., Micela, G., and Sciortino, S. 1997b *ApJ*, 483, 370

- Daniel, K. J., Linsky, J. L. and Gagné, M. 2002, *ApJ*, 578, 486
- Deacon, N. R. and Hambly, N. C. 2004, *A&A*, 416, 125
- Evans, N. R., Tingle, E., Bond, H. E., Schaefer, G., Karovska, M., Mason, B., DePasquale, J., Pillitteri, I., Wolk, S., Guinan, E., and Engle, S. 2012, *AAS* 219, #444.
- Favata, F. and Micela, G. 2003, *SpSci Rev.* 108, 577.
- Güdel, M., Guinan, E. F., and Skinner, S. L. 1997, *ApJ*. 483, 947
- Güdel, M. 2004, *AApRv*, 12, 71
- Jeffries, R. D., Evans, P. A., Pye, J. P., and Briggs, K. R. 2006, *MNRAS*, 367, 781
- Lodieu, N. Deacon, N. R., Hambly, N. C., and Boudreault, S. 2012, *MNRAS*, in press (astro-ph 1207.6978)
- Megeath, S. T. et al. 2012, arXiv:1209.3826)
- Meynet, G., Mermilliod, J.-C., and Maeder, A. 1993, *A&AS*, 98, 477
- Pallavicini, R., Francioscini, E., and Randich, S. 2004, *Mem S. A. It.*, 75, 434
- Pillitteri, I., Micela, G., Sciortino, S., Damiani, F., and Harnden, F. R. 2004, *A&A*, 421, 175
- Prosser, C. F. 1992, *AJ*, 103, 488
- Prosser, C. F., Randich, S., Stauffer, J. R., Schmitt, J. H. M. M., and Simon, T. 1996, *AJ*, 112, 1570
- Prosser, C. F., and Randich, S. 1998, *AN*, 319, 201 (PRS)
- Prosser, C. F., Randich, S., and Simon, T. 1998, *AN*, 319, 215
- Randich, S., Schmitt, J. H. M. M., Prosser, C. F., and Stauffer, J. R. 1996, *A&A*, 305, 785
- Siess, L., Dufour, E., and Forestini, M. 2000 *A&A*, 358, 593
- Stauffer, J. R., Barrado y Navascues, D., Bouvier, J., Morrison, H. L., Harding, P., Luhman, K. L., Stanke, T., McCaughrean, M., Terndrup, D. M., Allen, L., and Assouad, P. 1999, *ApJ*, 527, 219
- Telleschi, A., Guedel, M., Briggs, K., Audard, M., Ness, J.-U., and Skinner, S. L. 2005, *ApJ*, 622, 653.
- Wolk, S. J., Harnden, F. R., Flaccomio, E., Micela, G., Favata, F., Shang, H., and Feigelson, E. D. 2005, *ApJS*, 160, 423

Table 5: List of X-ray sources detected in EPIC-*XMM-Newton* image.

ID	R.A.	Dec.	Offaxis	Significance	Rate	Exp. Time
	(J2000)	(J2000)	'	σ_{bkg}	ct ks ⁻¹	ks
1	03:26:37.9	48:37:28.9	15.	15.7	5.55	48.3
2	03:25:43.7	48:38:32.4	14.	7.76	1.63	50.7
3	03:26:43.6	48:38:47.7	14.	6.75	1.66	57.3
4	03:26:01.3	48:39:10.1	12.	21.7	4.83	59.9
5	03:25:50.9	48:39:22.2	13.	29.4	7.41	57.4
6	03:25:53.0	48:40:30.2	11.	23.6	5.10	65.1
7	03:25:37.7	48:41:43.5	11.	14.8	2.79	63.7
8	03:26:54.5	48:42:17.0	12.	5.31	0.423	72.5
9	03:25:54.7	48:42:28.4	9.4	7.77	1.48	78.0
10	03:26:14.3	48:42:39.6	9.0	33.6	6.19	87.3
11	03:26:59.1	48:42:45.1	12.	60.4	16.5	73.9
12	03:26:24.1	48:42:46.3	9.2	9.78	1.35	88.1
13	03:26:41.3	48:43:18.9	10.	8.97	1.59	87.5
14	03:26:34.0	48:43:44.8	9.0	6.56	1.05	92.5
15	03:26:45.5	48:43:46.0	10.	20.9	3.34	77.4
16	03:26:41.5	48:43:56.6	9.5	5.43	0.459	91.3
17	03:25:29.8	48:44:00.1	9.8	5.89	1.18	68.8
18	03:26:18.4	48:44:06.8	7.7	4.90	0.396	98.5
19	03:26:22.6	48:44:20.2	7.7	5.95	0.435	103.
20	03:26:01.7	48:44:35.7	7.1	11.0	1.03	99.9
21	03:26:12.3	48:44:37.2	7.0	6.29	0.512	98.1
22	03:26:52.7	48:44:38.3	10.	5.96	0.512	89.6
23	03:27:16.4	48:44:43.2	13.	13.0	2.85	69.8
24	03:26:47.2	48:45:14.9	9.1	5.13	0.562	96.0
25	03:25:47.2	48:45:15.7	7.2	6.32	0.809	88.4
26	03:26:41.4	48:45:23.3	8.4	6.94	0.773	103.
27	03:25:56.5	48:45:40.6	6.2	5.34	0.399	105.
28	03:25:13.8	48:45:56.4	10.	5.52	1.27	56.2
29	03:25:27.2	48:46:03.6	8.6	15.1	1.45	74.3
30	03:27:05.5	48:46:20.4	11	11.9	2.22	86.8
31	03:25:26.3	48:46:28.9	8.5	6.38	0.483	75.7
32	03:26:40.8	48:46:38.7	7.4	24.2	4.84	55.7
33	03:25:23.0	48:46:58.3	8.7	10.5	1.23	71.4
34	03:27:02.8	48:47:07.7	10.	33.0	6.97	93.4
35	03:25:32.0	48:47:24.2	7.2	11.0	1.39	59.6
36	03:26:50.2	48:47:33.3	8.1	182.	63.3	111.
37	03:26:53.8	48:47:34.4	8.6	11.2	0.99	108.
38	03:26:11.1	48:47:45.8	3.9	7.64	0.512	131.
39	03:27:09.3	48:47:48.2	11.	9.50	1.71	84.7
40	03:25:35.9	48:48:05.7	6.3	6.23	0.521	96.1
41	03:26:04.2	48:48:08.5	3.5	224.	78.7	129.
42	03:24:58.9	48:48:12.8	12.	94.7	48.1	52.7
43	03:27:16.7	48:48:39.9	12.	6.89	0.861	82.1
44	03:25:54.4	48:48:49.2	3.5	6.36	0.571	119.
45	03:26:32.9	48:48:52.0	5.0	6.41	0.355	136.
46	03:27:10.9	48:49:00.3	11.	9.67	0.888	90.4
47	03:26:30.1	48:49:22.2	4.3	8.51	0.527	140
48	03:25:07.1	48:49:25.4	10.	15.4	3.26	52.4

Table 6: List of sources with 2MASS match and parameters from best fit modeling of X-ray spectra.

ID	R.A. (J2000)	Dec. (J2000)	2MASS ID	J mag	H mag	K mag	kT keV	E.M. cm^{-3}	$\log f_X$ $\text{erg s}^{-1} \text{cm}^{-2}$	$\log L_X$ erg s^{-1}
4	03:26:01.3	48:39:09.7	03260131+4839097	12.60	11.92	11.69	0.76	51.73	-13.8	28.8
10	03:26:14.2	48:42:38.3	03261419+4842382	12.48	11.80	11.55	0.89	51.92	-13.6	29.0
19	03:26:22.7	48:44:20.1	03262270+4844201	12.77	12.31	12.12	0.86	50.65	-14.9	27.7
22	03:26:52.6	48:44:37.9	03265263+4844378	11.10	10.77	10.76	0.88	51.06	-14.4	28.1
42	03:24:58.8	48:48:14.7	03245884+4848147	16.47	15.69	14.52	–	–	–	–
33	03:25:23.0	48:46:56.2	03252295+4846562	13.64	13.04	12.78	0.81	51.24	-14.3	28.2
35	03:25:31.8	48:47:21.4	03253182+4847213	13.80	13.18	12.98	0.81	51.38	-14.1	28.4
25	03:25:47.2	48:45:13.6	03254715+4845136	13.31	12.87	12.72	0.18	53.95	-11.9	30.7
27	03:25:56.6	48:45:38.1	03255664+4845381	15.65	14.90	14.67	–	–	–	–
41	03:26:04.2	48:48:07.1	03260421+4848070	9.49	9.21	9.16	0.64	53.17	-12.4	30.2
38	03:26:11.1	48:47:45.0	03261110+4847450	15.02	14.37	14.04	–	–	–	–
32	03:26:40.8	48:46:36.8	03264075+4846368	8.76	8.58	8.57	0.47	52.18	-13.4	29.1
26	03:26:41.2	48:45:21.0	03264121+4845210	14.6	13.86	13.67	–	–	–	–
36	03:26:50.1	48:47:32.1	03265010+4847320	9.20	9.01	8.89	0.64	53.10	-12.4	30.1
39	03:27:09.4	48:47:49.2	03270936+4847491	12.03	11.63	11.56	0.53	52.62	-13.1	29.4
30	03:27:05.7	48:46:20.1	03270565+4846201	16.70	16.05	16.33	–	–	–	–
68	03:24:49.7	48:52:18.4	03244971+4852183	10.11	9.72	9.59	0.90	52.89	-12.6	29.9
48	03:25:07.2	48:49:26.0	03250721+4849260	13.12	12.4	12.20	–	–	–	–
65	03:25:12.3	48:52:05.3	03251232+4852052	9.77	9.56	9.47	0.53	51.69	-13.9	28.7
59	03:25:24.3	48:51:40.8	03252428+4851407	12.38	12.02	11.92	0.34	52.07	-13.6	28.9
63	03:25:50.7	48:52:05.3	03255074+4852052	13.20	12.72	12.59	0.54	51.69	-13.9	28.7
58	03:26:01.0	48:51:30.9	03260103+4851309	15.37	14.97	14.59	–	–	–	–
47	03:26:30.0	48:49:20.9	03262999+4849209	14.08	13.49	13.22	0.73	50.92	-14.6	27.9
52	03:26:16.4	48:50:28.4	03261639+4850284	10.81	10.32	10.21	0.77	52.45	-13.1	29.5
67	03:26:41.3	48:52:16.1	03264130+4852160	11.83	11.54	11.44	0.65	51.71	-13.8	28.7
51	03:27:02.4	48:50:19.4	03270241+4850193	13.18	12.56	12.30	0.58	51.14	-14.4	28.1
62	03:27:39.6	48:51:54.0	03273962+4851539	12.13	11.72	11.60	0.60	51.49	-14.0	28.5
74	03:24:48.4	48:53:19.9	03244838+4853199	10.08	9.55	9.42	0.96	53.06	-12.5	30.1
82	03:25:36.1	48:55:57.4	03253612+4855573	13.52	12.93	12.57	0.82	51.32	-14.2	28.4
77	03:25:46.0	48:54:10.0	03254597+4854100	15.95	15.21	14.99	–	–	–	–
69	03:26:02.8	48:52:59.2	03260275+4852591	16.26	15.64	15.12	–	–	–	–
71	03:27:05.1	48:53:04.5	03270505+4853044	10.57	9.981	9.78	0.97	51.40	-12.7	29.8
75	03:27:11.2	48:53:60.0	03271116+4853599	14.62	13.87	13.67	–	–	–	–
90	03:25:10.4	48:59:45.4	03251041+4859453	12.59	12.01	11.75	1.01	52.25	-13.3	29.3
85	03:25:28.7	48:57:51.5	03252866+4857515	11.43	10.98	10.84	0.96	52.11	-13.4	29.1
87	03:25:28.9	48:58:14.3	03252893+4858143	14.53	13.99	13.88	–	–	–	–
86	03:27:24.9	48:58:11.9	03272491+4858118	13.53	12.88	12.62	0.97	52.03	-13.5	29.0
92	03:26:06.0	49:00:06.4	03260595+4900064	15.64	14.79	14.44	34	52.58	-12.8	29.8
96	03:26:27.6	49:02:12.4	03262764+4902123	10.77	10.26	10.11	0.94	52.75	-12.8	29.8